nature structural & molecular biology

Dynamics of the unbound head during myosin V processive translocation

Alexander R Dunn & James A Spudich

Myosin V moves cargoes along actin filaments by walking hand over hand. Although numerous studies support the basic hand-over-hand model, little is known about the fleeting intermediate that occurs when the rear head detaches from the filament. Here we use submillisecond dark-field imaging of gold nanoparticle–labeled myosin V to directly observe the free head as it releases from the actin filament, diffuses forward and rebinds. We find that the unbound head rotates freely about the lever-arm junction, a trait that likely facilitates travel through crowded actin meshworks.

Myosin V (M5) functions as a dimer and moves processively along actin using a hand-over-hand mechanism[1]. In this mechanism, the rear head must release the actin filament and travel forward before rebinding. It is not known whether the temporarily free head is constrained or is free to rotate, or how quickly it rebinds the actin filament. Some models require the free head to remain very near the actin filament and even interact with each actin monomer along one protofilament[2,3]. In addition, the rate of free-head rebinding affects processivity, and the degree of conformational freedom probably affects the ease with which M5 switches between actin filaments.

To address unanswered mechanistic questions about M5, we sought to track one of the two lever arms with millisecond or better time resolution. Accordingly, we attached single gold nanoparticles to the lever arm of dimeric M5 derived from chicken (**Fig. 1a**). Gold nanoparticles scatter light efficiently, and under dark-field illumination they appear as bright spots against a dark background, analogous to single fluorophores. Unlike fluorophores, the photon flux is not limited by the excited state lifetime, bleaching or blinking. It is therefore possible to track gold nanoparticles with submillisecond time resolution[4].

Dimeric M5 was expressed in the presence of calmodulin (M5cam) or calmodulin plus the essential light chain LC1sa (M5elc) (**Supplementary Fig. 1** online). When present, LC1sa replaces calmodulin at the lever-arm binding site closest to the catalytic domain. Unless noted, data are reported for M5elc. M5 was labeled with biotinylated calmodulin and conjugated to 40-nm-diameter streptavidin-coated gold nanoparticles, unless otherwise noted (**Supplementary Methods** online). The resulting M5-gold conjugates were imaged using darkfield microscopy with frame rates up to 3,125 Hz. Single particles moved directionally along surface-immobilized actin filaments (**Fig. 1b** and **Supplementary Video 1** online).

As with single-molecule fluorescence experiments[5], we commonly observed alternating steps of 74.7 ± 0.9 (s.e.m.) and 0 nm (**Fig. 1b**). We also observed alternating steps of 53 and 21 nm (**Supplementary Fig. 2** online) or of 40 and 30 nm (data not shown), which result from gold particles attached to calmodulins higher up on the lever arm[5]. Both the size[5] and rate[6] of the 74-nm steps match previously reported values, indicating that the attachment of the gold particle does not perturb the behavior of the motor (**Supplementary Fig. 3** online).

Closer inspection of the 74-nm step reveals an intermediate (**Fig. 1c** and **Supplementary Fig. 4** online) that corresponds to a one-head-bound state (**Fig. 2**). The intermediate breaks the step into 49- and 25-nm components, defined relative to the data points recorded during the 16 ms before and after the step (**Fig. 2a**).

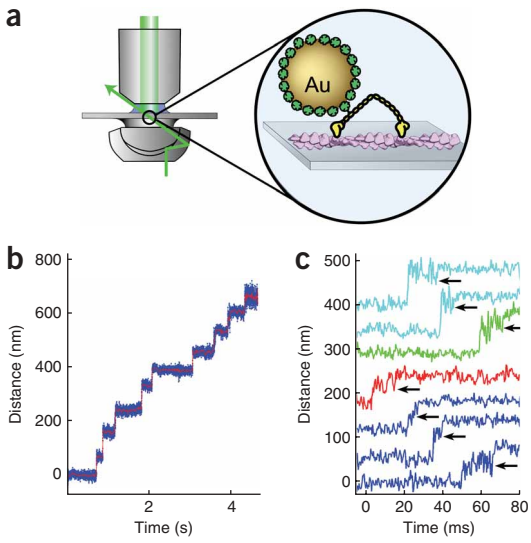

Figure 1 Tracking the motion of the M5 lever arm with millisecond time resolution. (**a**) A M5 dimer is labeled with a gold nanoparticle on one of its lever arms through a biotin-streptavidin linkage. The M5-gold conjugate walks along surface-immobilized actin. Light scattered by the gold particle is collected by the objective. (**b**) Sample data trace; 40 nm gold, 3 μM ATP. Frames were taken every 0.32 ms (blue); a 6.4-ms sliding average is shown in red. (**c**) Sample 49-nm substeps; 3,125 Hz, 40 nm gold. The end of the substep is indicated by an arrow. Each color corresponds to an individual molecule. Note the increase in variance during the substep.

Stanford University School of Medicine, Beckman Center, 279 Campus Drive, Stanford, California 94305-5307, USA. Correspondence should be addressed to J.A.S. (jspudich@stanford.edu).

Received 17 October 2006; accepted 22 January 2007; published online 11 February 2007; corrected online 18 February 2007 (details online); doi:10.1038/nsmb1206

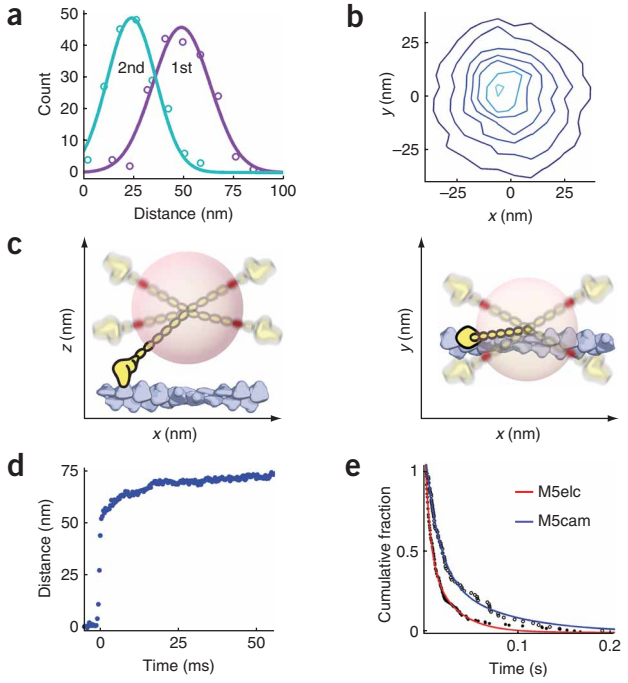

Figure 2 Characterization of the one-head-bound intermediate. (**a**) The 74-nm displacement consists of a 49 ± 1 nm (1st) followed by a 25 ± 1 nm (2nd) substep ($n = 182$). (**b**) Contour plot in the x and y directions of data points collected during the intermediate. The distribution can be fit by a two-dimensional Gaussian function with 18 nm s.d. in x and y (data from 194 events). The fit is radially symmetric to within 5%. (**c**) In a simple model, the gold particle follows the labeled calmodulin (red) as it rotates freely in the x, y and z directions during the intermediate, resulting in the observed s.d. increase. (**d**) Trace resulting from 231 aligned and averaged steps. The rise to 49 nm is too fast to be resolved. (**e**) Distribution of substep dwell times, plotted as the cumulative fraction for M5elc ($n = 194$) and M5cam ($n = 87$).

To determine the extent of motion of the free head both along the actin filament long axis (the x direction) and perpendicular to that axis (the y direction), we measured the change in variance in both x and y during the substep compared with that before or after the substep. The standard deviation (s.d.) of the 49-nm substep shows a radially symmetric increase (18 nm; **Fig. 2b**) relative to the s.d. immediately before or after the substep (12 nm; **Supplementary Fig. 5** online), consistent with free diffusion of the detached head about the junction between lever arms (**Fig. 2c** and **Supplementary Fig. 6** online). Calculations based on the simple model that the gold particle sweeps out the surface of a sphere are consistent with the particle being attached ~20 nm from the lever arm junction, in reasonable agreement with the anticipated length of the lever arm (**Supplementary Methods**). Other models—for instance, rotation solely in the xy plane—can in principle fit the data (**Supplemental Methods**). However, no obvious physical model results in this scenario, whereas free rotation requires only a short, unconstrained peptide linker to act as a swivel. About half of the runs end in a 49-nm step and an increased s.d., suggesting that these runs terminate when the free head cannot rebind (**Supplementary Methods**).

In addition to the 49-nm displacement along the actin filament, the intermediate shows a lateral (perpendicular) displacement of 4 to 8 nm to the left, defined relative to the myosin direction of travel (**Supplementary Fig. 7** online). This displacement is roughly consistent with the lateral angular displacements reported previously[7] and may reflect an off-axis component of the power stroke, in keeping with the observation that myosin V walks in a left-handed spiral[8].

However, we cannot rule out the possibility that this observation is an artifact resulting from the gold-myosin attachment.

Formation of the 49-nm substep is faster than our detection limit at 3,125 frames s^{-1} (**Fig. 2d**). The 49-nm substep is consistent with the simultaneous release of ~10 nm of intramolecular tension[9], a 20-nm power stroke[10] and ~20 nm of diffusion such that the new average position of the bead corresponds to the lever-arm junction (**Fig. 3a–d**). Our data apparently conflict with models containing a millisecond or longer pause between the release of the rear head and the lever-arm swing[11], as well as models where the free head closely tracks the actin filament[2].

A cumulative lifetime plot for the one-head-bound state shows a fast decay that is fit by a single exponential and a slower tail owing to intermediates whose rebinding is slowed by local steric hindrance (**Fig. 2e** and **Supplementary Methods**). Free-head rebinding is faster

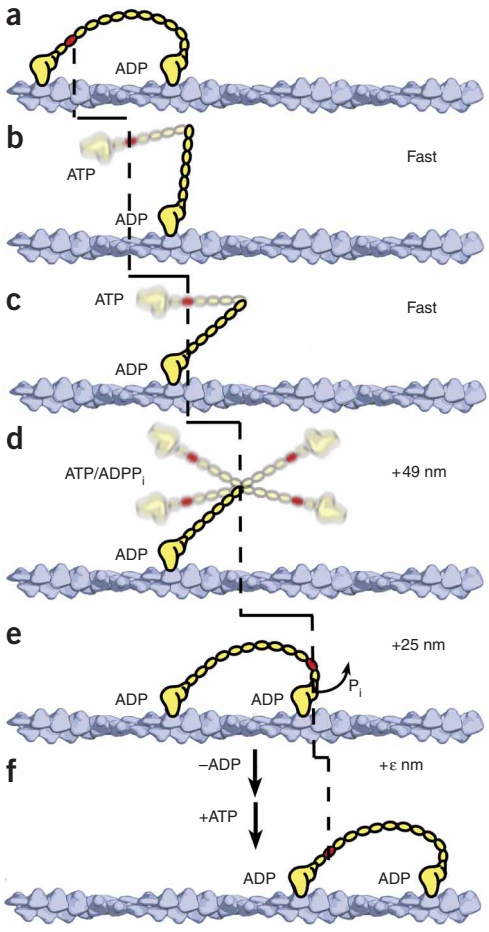

Figure 3 A myosin V model mechanism. The gold nanoparticle follows the labeled calmodulin (*red*). (**a**) The rear head binds ATP and detaches from actin. (**b–d**) The 49-nm substep results from the release of intramolecular tension (**b**), a lever-arm swing (**c**), and free diffusion of the unbound head such that the average gold particle position reflects that of the lever-arm junction (**d**). (**e**) The free head rebinds, resulting in a second 25-nm substep. (**f**) The rear head releases ADP, binds ATP and steps forward, resulting in a small translocation (ε).

for M5elc ($180 \pm 50\ s^{-1}$) than for M5cam ($60 \pm 15\ s^{-1}$), consistent with previously reported ensemble ATPase measurements[12]. In effect, the free head of M5cam has more time to find its next binding site, which could be an important variation *in vivo*.

We found that 100 mM 2,3-butanedione monoxime (BDM) slowed the rebinding rate to $80 \pm 13\ s^{-1}$. A previous study has reported the prolongation of a myosin V substep in the presence of BDM, attributing this to delay of the power stroke[11]. In our data, such a delay would be expected to break the 49-nm substep into displacements of 20 and ~30 nm. Instead, we see only a single, response-limited 49-nm substep (**Supplementary Fig. 8** online). We hypothesize that, at least under zero load and rate-limiting ATP concentrations, BDM inhibits the initial rebinding step.

Free-head rebinding is nearly irreversible, as indicated by examination of individual steps. In addition, 50 mM free sodium phosphate (P_i) had no discernable effect on the intermediate decay rate ($170 \pm 40\ s^{-1}$; **Supplementary Fig. 9** online). These observations suggest that phosphate release and a strong binding transition occur rapidly (**Fig. 3e**). A P_i release rate of $230\ s^{-1}$ has been reported[13], consistent with this model. We consider the measured M5elc free-head binding rate of $180\ s^{-1}$ a lower limit, given that the presence of the gold particle could conceivably slow rebinding. Our data are thus inconsistent with models containing slow ($\sim 5\ s^{-1}$) rebinding and phosphate release[14]. Added P_i slowed the rate of overall stepping to $1.0 \pm 0.1\ s^{-1}$ at 3 μM ATP, from $2.9\ s^{-1}$ measured in standard assay buffer. This inhibition was observed under rate-limiting ATP. Thus, P_i may inhibit ATP binding to the rear head.

We did not directly observe alternating steps of $74 - \varepsilon$ nm and ε nm (**Fig. 3f**), where ε is in the range of 6–10 nm, as reported earlier[15,16]. The simplest model consistent with our observation has a bent front lever arm, the so-called 'telemark' model[17]. This difference in data and resulting models should be interpreted with caution, as it may arise from differences in the myosin light-chain complement or other subtle effects (**Supplementary Methods**). EM studies support both bent[17] and straight[18] front lever arm models (**Supplementary Methods**). Further investigation will be necessary to definitively determine the state of the lead lever arm.

Our results are consistent with rapid phosphate release upon lead-head rebinding and local rotation about the pivot point in the catalytic domain, which leads to a strained leading head. Full rotation of the lever arm is prevented by intramolecular strain[9]. This picture of the lead head is consistent with results[19,20] and models[21] that indicate that the lead head, although robustly bound to actin, is not identical to a canonical rigor-bound head.

Our proposed model (**Fig. 3**) is attractive in its simplicity and appears sufficient to describe the behavior of myosin V under our conditions: zero load and rate-limiting ATP concentrations. It is conceivable that more complicated, bifurcating mechanisms[11,14] may be necessary to describe the behavior of myosin V under different nucleotide conditions or under applied load.

The conformational flexibility of the free head is probably an advantage when traversing the tangled actin meshwork in the cell cortex. Our data also indicate that the lead head rebinds the actin filament relatively quickly, a necessary trait for processive stepping. Thus, the properties of the one-head-bound intermediate successfully counterbalance processivity with the ability to step around obstacles in a complex environment. Both myosin V[22] and myosin VI[23] bind a variety of light chains *in vivo*. The different free-head rebinding rates we observed for M5elc and M5cam lead us to speculate that light-chain composition may tailor the behavior of unconventional myosins *in vivo*[24].

Note: Supplementary information is available on the Nature Structural & Molecular Biology website.

ACKNOWLEDGMENTS

We thank R. Vale (University of California, San Francisco) for the loan of the dark-field condenser and Z. Bryant and S. Churchman for insightful commentary. A.R.D. is a Jane Coffin Childs Postdoctoral Fellow. J.A.S. is supported by grant GM33289 from the US National Institutes of Health.

COMPETING INTERESTS STATEMENT

The authors declare that they have no competing financial interests.

Published online at http://www.nature.com/nsmb/
Reprints and permissions information is available online at http://npg.nature.com/reprintsandpermissions

1. Sellers, J.R. & Veigel, C. *Curr. Opin. Cell Biol.* **18**, 68–73 (2006).
2. Kitamura, K., Tokunaga, M., Iwane, A.H. & Yanagida, T. *Nature* **397**, 129–134 (1999).
3. Watanabe, T.M. *et al. Proc. Natl. Acad. Sci. USA* **101**, 9630–9635 (2004).
4. Yasuda, R., Noji, H., Yoshida, M., Kinosita, K., Jr. & Itoh, H. *Nature* **410**, 898–904 (2001).
5. Yildiz, A. *et al. Science* **300**, 2061–2065 (2003).
6. De La Cruz, E.M., Wells, A.L., Rosenfeld, S.S., Ostap, E.M. & Sweeney, H.L. *Proc. Natl. Acad. Sci. USA* **96**, 13726–13731 (1999).
7. Forkey, J.N., Quinlan, M.E., Shaw, M.A., Corrie, J.E. & Goldman, Y.E. *Nature* **422**, 399–404 (2003).
8. Ali, M.Y. *et al. Nat. Struct. Biol.* **9**, 464–467 (2002).
9. Veigel, C., Schmitz, S., Wang, F. & Sellers, J.R. *Nat. Cell Biol.* **7**, 861–869 (2005).
10. Veigel, C., Wang, F., Bartoo, M.L., Sellers, J.R. & Molloy, J.E. *Nat. Cell Biol.* **4**, 59–65 (2002).
11. Uemura, S., Higuchi, H., Olivares, A.O., De La Cruz, E.M. & Ishiwata, S. *Nat. Struct. Mol. Biol.* **11**, 877–883 (2004).
12. De La Cruz, E.M., Wells, A.L., Sweeney, H.L. & Ostap, E.M. *Biochemistry* **39**, 14196–14202 (2000).
13. Rosenfeld, S.S. & Sweeney, H.L. *J. Biol. Chem.* **279**, 40100–40111 (2004).
14. Baker, J.E. *et al. Proc. Natl. Acad. Sci. USA* **101**, 5542–5546 (2004).
15. Syed, S., Snyder, G.E., Franzini-Armstrong, C., Selvin, P.R. & Goldman, Y.E. *EMBO J.* **25**, 1795–1803 (2006).
16. Toprak, E. *et al. Proc. Natl. Acad. Sci. USA* **103**, 6495–6499 (2006).
17. Walker, M.L. *et al. Nature* **405**, 804–807 (2000).
18. Burgess, S. *et al. J. Cell Biol.* **159**, 983–991 (2002).
19. Purcell, T.J., Sweeney, H.L. & Spudich, J.A. *Proc. Natl. Acad. Sci. USA* **102**, 13873–13878 (2005).
20. Olivares, A.O., Chang, W., Mooseker, M.S., Hackney, D.D. & De La Cruz, E.M. *J. Biol. Chem.* **281**, 31326–31336 (2006).
21. De La Cruz, E.M. & Ostap, E.M. *Curr. Opin. Cell Biol.* **16**, 61–67 (2004).
22. Espindola, F.S. *et al. Cell Motil. Cytoskeleton* **47**, 269–281 (2000).
23. Frank, D.J. *et al. J. Biol. Chem.* **281**, 24728–24736 (2006).
24. Snider, J. *et al. Proc. Natl. Acad. Sci. USA* **101**, 13204–13209 (2004).